Development of EMD-Based Denoising Methods Inspired by Wavelet Thresholding

Yannis Kopsinis, *Member, IEEE*, and Stephen McLaughlin, *Senior Member, IEEE*

***Abstract*—One of the tasks for which empirical mode decomposition (EMD) is potentially useful is nonparametric signal denoising, an area for which wavelet thresholding has been the dominant technique for many years. In this paper, the wavelet thresholding principle is used in the decomposition modes resulting from applying EMD to a signal. We show that although a direct application of this principle is not feasible in the EMD case, it can be appropriately adapted by exploiting the special characteristics of the EMD decomposition modes. In the same manner, inspired by the translation invariant wavelet thresholding, a similar technique adapted to EMD is developed, leading to enhanced denoising performance.**

***Index Terms*—Empirical mode decomposition (EMD), signal denoising, wavelet thresholding.**

I. Introduction

THE empirical mode decomposition (EMD) method [3] is an algorithm for the analysis of multicomponent signals [4] that breaks them down into a number of amplitude and frequency modulated (AM/FM) zero-mean signals, termed intrinsic mode functions (IMFs). In contrast to conventional decomposition methods such as wavelets, which perform the analysis by projecting the signal under consideration onto a number of predefined basis vectors, EMD expresses the signal as an expansion of basis functions that are signal-dependent and are estimated via an iterative procedure called sifting.

Although many attempts have been made to improve the understanding of the way EMD operates or to enhance its performance (see, for example, [5]–[9]), EMD still lacks a sound mathematical theory and is essentially described by an algorithm. However, partly due to the fact that it is easily and directly applicable and partly because it often results in interesting and useful decomposition outcomes, it has found a vast number of diverse applications such us biomedical [10], [11], watermarking [12], and audio processing [13] to name a few.

Apart from the specific applications of EMD listed above, a more generalized task in which EMD can prove useful is signal denoising. In this paper, inspired by standard wavelet thresholding and translation invariant thresholding, a number of EMD-based denoising techniques are developed[1] and tested in different signal scenarios and white Gaussian noise. It is shown that although the main principles between wavelet and EMD thresholding are the same, in the case of EMD, the thresholding operation has to be properly adapted in order to be consistent with the special characteristics of the signal modes resulting from EMD.

The remainder of the paper is organized as follows. Section II provides a brief description of EMD, and the notation required in the rest of the paper is introduced. In Section III the major concepts of wavelet thresholding as well as conventional EMD denoising are described. Section IV explores the possibility of adapting the wavelet thresholding principles in thresholding the decomposition modes of EMD directly. Consequently, three novel EMD-based hard and soft thresholding strategies are presented. The performance evaluation of the novel denoising techniques is illustrated in Section V, and the final conclusions are drawn in Section VI.

II. EMD: A Brief Description and Notation

EMD [3] adaptively decomposes a multicomponent signal [4] $x(t)$ into a number L of the so-called IMFs $h^{(i)}(t)$, $1 \leq i \leq L$

$$x(t) = \sum_{i=1}^{L} h^{(i)}(t) + d(t) \tag{1}$$

where $d(t)$ is a remainder that is a non-zero-mean slowly varying function with only few extrema. Each one of the IMFs, say, the ith one $h^{(i)}(t)$, is estimated with the aid of an iterative process, called sifting, applied to the residual multicomponent signal

$$x^{(i)}(t) = \begin{cases} x(t), & i = 1 \\ x(t) - \sum_{j=1}^{i-1} h^{(j)}(t), & i \geq 2. \end{cases} \tag{2}$$

The sifting process used in this paper is the standard one [3]. According to this, during the $(n+1)$th sifting iteration, the temporary IMF estimate $h_n^{(i)}(t)$ is improving according to the following steps.[2]

1) Find the local maxima and minima of $h_n^{(i)}(t)$.
2) Interpolate, using natural cubic splines, along the points of $h_n^{(i)}(t)$ estimated in the first step in order to form an upper and a lower envelope.
3) Compute the mean of the two envelopes.

Manuscript received February 05, 2008; accepted December 08, 2008. First published January 23, 2009; current version published March 11, 2009. The associate editor coordinating the review of this manuscript and approving it for publication was Prof. Gerald Schuller. This work was supported by the EPSRC under their Basic Technology Programme as part of the BIAS consortium. Part of this paper has appeared in the *Proceedings of the Sixteenth European Signal Processing Conference*, Lausanne, Switzerland, August 25–29, 2008 and the *Proceedings of the First IAPR Workshop Cognitive Information Processing*, Santorini, Greece, June 9–10, 2008, pp. 42–47.

The authors are with the Institute for Digital Communications, School of Engineering and Electronics, University of Edinburgh, EH9 3JL Edinburgh, U.K. (e-mail: y.kopsinis@ed.ac.uk; Steve.McLaughlin@ed.ac.uk).

Color versions of one or more of the figures in this paper are available online at http://ieeexplore.ieee.org.

Digital Object Identifier 10.1109/TSP.2009.2013885

[1]Matlab scripts for all the novel denoising in methods developed in this paper can be downloaded from http://www.see.ed.ac.uk/~ykopsini/emd/emd.html.

[2]For the first iteration, $x^{(i)}(t)$ is used as temporary IMF estimate $h_1(t)$.

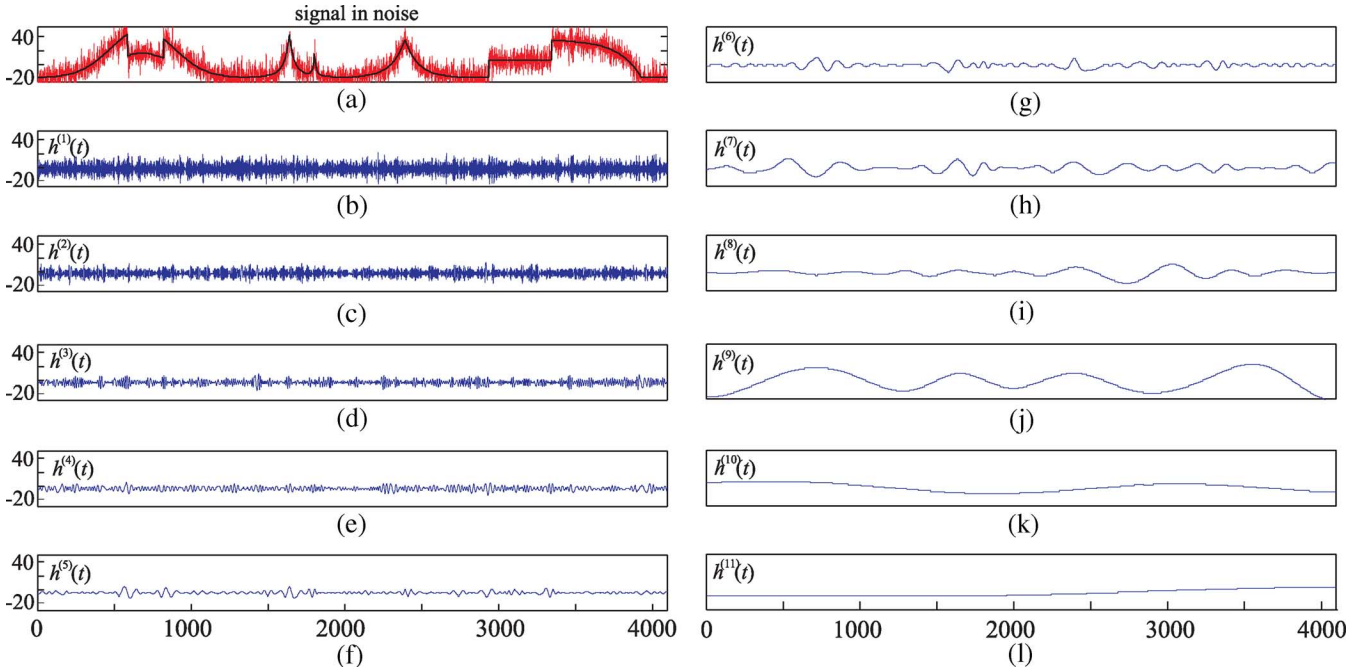

Fig. 1. Empirical mode decomposition of the noisy signal shown in (a).

4) Obtain the refined estimate $h_{n+1}^{(i)}(t)$ of the IMF by subtracting the mean found in the previous step from the current IMF estimate $h_n^{(i)}(t)$.
5) Proceed from step 1) again unless a stopping criterion has been fulfilled.

The sifting process is effectively an empirical but powerful technique for the estimation of the mean $m^{(i)}(t)$ of the residual multicomponent signal $x^{(i)}(t)$ locally, a quantity that we term *total local mean*.[3] Although the notion of the total local mean is somewhat vague, especially for multicomponent signals, in the EMD context it means that its subtraction from $x^{(i)}(t)$ will lead to a signal, which is actually the corresponding IMF, i.e., $h^{(i)}(t) = x^{(i)}(t) - m^{(i)}(t)$, that is going to have the following properties.

1) Zero mean.
2) All the maxima and all the minima of $h^{(i)}(t)$ will be positive and negative, respectively.

Often, but not always, the IMFs resemble sinusoids that are both amplitude and frequency modulated.

By construction, the number of, say, $N(i)$ extrema of $h^{(i)}(t)$ positioned at time instances $\boldsymbol{r}^{(i)} = [r_1^{(i)}, r_2^{(i)}, \ldots, r_{N(i)}^{(i)}]$ and the corresponding IMF points $h^{(i)}(r_j^{(i)}), j = 1, \ldots, N(i)$ will alternate between maxima and minima, i.e., positive and negative values. As a result, in any pair of extrema, $\boldsymbol{r}_j^{(i)} = [h^{(i)}(r_j^{(i)}), h^{(i)}(r_{j+1}^{(i)})]$ corresponds to a single zero-crossing $z_j^{(i)}$. Depending on the IMF shape, the number of zero-crossings can be either[4] $N(i)$ or $N(i)-1$. Moreover, each IMF, say, the one of order i, has fewer extrema than all the lower order IMFs, $j = 1, \ldots, i-1$, leading to fewer and fewer oscillations as the IMF order increases. In other words, each IMF occupies lower frequencies locally in the time–frequency domain than its preceding ones.

Fig. 1 depicts as an example the EMD of the well-studied piecewise-regular signal [14] [Fig. 1(a)] corrupted by white Gaussian noise corresponding to 5 dB signal-to-noise power ratio (SNR). EMD results in ten IMFs and the final remainder $h^{(11)}(t)$, which are depicted in Fig. 1(b)–(l).

III. Signal Denoising

Digital signal denoising can be described as follows. Having a sampled noisy signal $x(t)$ given by

$$x(t) = \bar{x}(t) + \sigma n(t), \quad t = 1, 2, \ldots, N \tag{3}$$

where $\bar{x}(t)$ is the noiseless signal and $n(t)$ are independent random variables Gaussian distributed $\mathcal{N}(0,1)$, produce an estimate $\tilde{x}(t)$ of signal $\bar{x}(t)$. Noise variance σ can be known or unknown, and the denoising methods can be categorized as parametric or nonparametric depending on whether a predefined parametric model of $\bar{x}(t)$ has been adopted or not. In this paper, the focus is on the nonparametric framework where the best known candidates are denoising techniques based on wavelet decomposition [14]–[16]. Moreover, the novelty of this paper lies in the introduction of new nonparametric thresholding techniques applied to the decomposition modes resulting from EMD instead of the wavelet components. As will be seen, thresholding in EMD is not a straightforward application of the concepts used in wavelet thresholding.

A. Wavelet Based Denoising

Employing a chosen orthonormal wavelet basis, an orthogonal $N \times N$ matrix $\boldsymbol{W}$ is appropriately built [17], which in turn leads to the discrete wavelet transform (DWT)

$$\boldsymbol{c} = \boldsymbol{W}\boldsymbol{x}$$

[3]The term *local mean* would be more appropriate, but we avoid it here because it is usually used to describe the mean of the two envelopes of the second step of the sifting iteration.

[4]The end points of the signal are counted as extrema.

where $\boldsymbol{x} = [x(1), x(2), \ldots, x(N)]$ and $\boldsymbol{c} = [c_1, c_2, \ldots, c_N]$ contains the resultant wavelet coefficients. Due to the orthogonality of matrix $\boldsymbol{W}$, any wavelet coefficient c_i follows a normal distribution with variance σ and mean the corresponding coefficient value $\bar{c}_i$ of the DWT of the noiseless signal $\bar{x}(t)$. Provided that the signal under consideration is sparse in the wavelet domain, which is usually the case, then the DWT is expected to distribute the total energy of $\bar{x}(t)$ in only a few wavelet components lending themselves to high amplitudes. As a result, the amplitude of most of the wavelet components is attributed to noise only. The fundamental reasoning of wavelet thresholding is to set to zero all the components that are lower than a threshold related to the noise level, i.e., $T = \sigma C$, where C is a constant, and then reconstruct the denoised signal $\tilde{x}(t)$ utilizing the high-amplitude components only. There are two major thresholding operators—hard and soft thresholding—defined by

$$\rho_T(y) = \begin{cases} y, & |y| > T \\ 0, & |y| \leq T \end{cases} \tag{4}$$

and

$$\rho_T(y) = \begin{cases} \operatorname{sgn}(y)\,(|y| - T), & |y| > T \\ 0, & |y| \leq T \end{cases} \tag{5}$$

respectively.

Using any one of the thresholding operators above, the estimated denoised signal is given by

$$\tilde{\boldsymbol{x}} = \boldsymbol{W}^T \tilde{\boldsymbol{c}} \tag{6}$$

where $\tilde{\boldsymbol{c}} = [\rho_T(c_1), \rho_T(c_2), \ldots, \rho_T(c_N)]$ and $\boldsymbol{W}^T$ denotes transposition of matrix $\boldsymbol{W}$. Apart from the standard wavelet thresholding described above, a number of modifications are investigated in Section V, including translation invariant thresholding [14] and Bayesian-based wavelet thresholding [15], [18].

With respect to the threshold selection, the universal threshold $T = \sigma\sqrt{2 \ln N}$ is a popular candidate. Such a threshold guarantees with high probability that all of the components attributed to noise will have lower amplitudes and, therefore, they will get thresholded. In this paper, multiples of the above threshold are used, and the standard deviation of the noise is estimated using a robust estimator based on the components median [14]

$$\hat{\sigma} = \frac{\operatorname{median}\left(|c_i| : i = 1, \ldots, N\right)}{0.6745}. \tag{7}$$

The specific standard deviation estimator leads to accurate estimates even if there are components attributed to signal. Lastly, it is usually beneficial to apply thresholding after a primary resolution level, leaving the coarse scales corresponding to low frequencies unthresholded. This parameter will be also taken into account in this paper.

Fig. 2(a)–(c) shows the noise-free estimates of the signal of Fig. 1(a) corrupted by noise using, from top to bottom, wavelet hard thresholding with universal threshold, translation invariant wavelet thresholding with universal threshold, and Bayesian-based wavelet thresholding. The numbers on the top left of the figures indicate the SNRs after the denoising procedure when the SNR is 5 dB before denoising. Note that this performance corresponds to a single arbitrary noise realization. Detailed, ensemble averaged performance results of the thresholding techniques above will be presented in Section V.

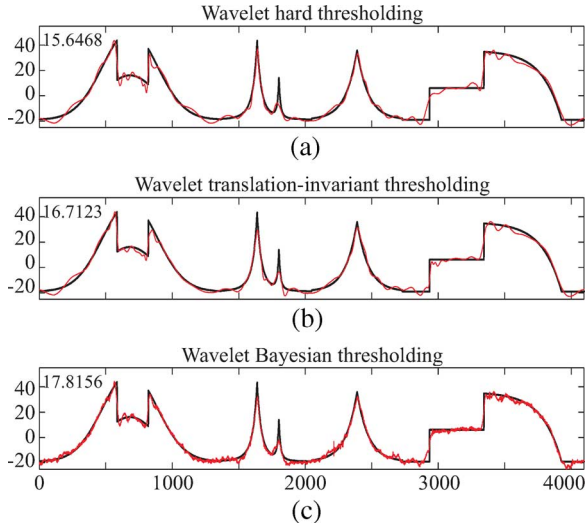

Fig. 2. Examples of wavelet-based denoising when SNR= 5 dB. The top-left numbers are the SNR values after denoising.

B. Conventional EMD Denoising

The first attempt at using EMD as a denoising tool emerged from the need to know whether a specific IMF contains useful information or primarily noise. Thus, significance IMF test procedures were simultaneously developed both by Flandrin *et al.* [5], [19] and Wu *et al.* [20], [21] based on the statistical analysis of modes resulting from the decomposition of signals solely consisting of fractional Gaussian noise and white Gaussian noise, respectively. The reasoning underlying the significance test procedure above is fairly simple but strong. If the energy of the IMFs resulting from the decomposition of a noise-only signal with certain characteristics is known, then in actual cases of signals comprising both information and noise following the specific characteristics, a significant discrepancy between the energy of a noise-only IMF and the corresponding noisy-signal IMF indicates the presence of useful information. In a denoising scenario, this translates to partially reconstructing the signal using only the IMFs that contain useful information and discarding those that carry primarily noise, i.e., the IMFs that share similar amounts of energy with the noise-only case.

In practice, the noise-only signal is never available in order to apply EMD and estimate the IMF energies, so the usefulness of the above technique relies on whether or not the energies of the noise-only IMFs can be estimated directly based on the actual noisy signal. The latter is usually the case due to a striking feature of EMD. Apart from the first noise-only IMF, the power spectra of the other IMFs exhibit self-similar characteristics akin to those that appear in any dyadic filter structure. As a result, the IMF energies E_k should linearly decrease in a semilog diagram of, e.g., $\log_2 E_k$ with respect to k for $k \geq 2$. It also turns out that the first IMF carries the highest amounts of

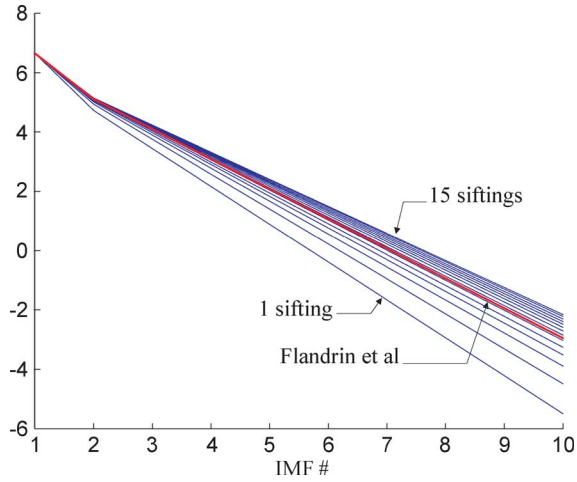

Fig. 3. Curves that link the estimated energies of the IMFs which correspond to EMDs using from one to 15 sifting iterations. The thick red line indicated as "Flandrin et al." corresponds to the β and ρ parameters proposed in [19].

energy. In this paper, the focus is on signals with white Gaussian noise. Then, the noise-only IMF energies can be approximated [19] according to

$$\hat{E}_k = \frac{E_1^2}{\beta}\rho^{-k}, \quad k = 2, 3, 4, \ldots \tag{8}$$

where E_1^2 is the energy of the first IMF and β, ρ are parameters that, for a specific EMD implementation, depend mainly on the number of sifting iterations used. These parameters can be estimated in one step based on a large number of independent noise realizations and their corresponding IMFs [19].

Fig. 3 shows the curves that link the estimated energies of the IMFs $k = 1, \ldots, 10$, based on model (8), where the parameters β and ρ correspond to EMDs using from one up to 15 sifting iterations. We observe that as the number of sifting iterations increases, the corresponding curves approach each other. This is in agreement with the analytically derived frequency responses of the equivalent filtering operations that correspond to EMDs with different number of sifting iterations in a two-sinusoids signal case [6]. Flandrin *et al.* [19] specifically proposed for the parameters β and ρ the values 0.719 and 2.01, respectively, that correspond to the curve drawn with a thick red line. We see that these parameters correspond to a curve that is representative by being close to an average of the "trend" that the rest of the energy curves exhibit. Hereafter, the IMF energy curve that corresponds to the later specification of β and ρ will be called *fixed* in order to coincide with the sifting dependent IMF energy curves.

Fig. 4 depicts the conventional denoising procedure and results when it is applied on the test signal of Fig. 1(a). On top, with a solid line, we see the semilog diagram (energies with respect to IMF number) of the corresponding IMFs [Fig. 1(b)–(l)], and the dashed line shows the results of the noise-only model of (8). We observe that, after the fifth IMF, the energies significantly diverge from the theoretical model, indicating the presence of significant amounts of no-noise signal. The partial signal reconstruction including only IMFs number 6 to 11 results in the denoised signal shown in Fig. 4.

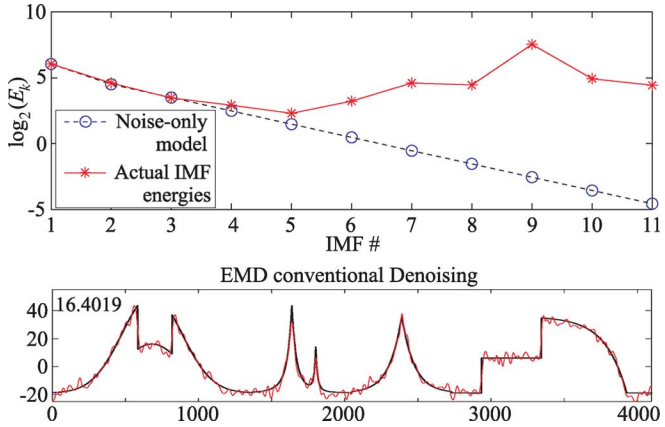

Fig. 4. (a) Theoretical noise-only model and actual IMF energies with respect to IMF number. (b) The resulted denoised signal when, for the reconstruction, IMFs number 6 to 11 are used only.

IV. IMF Thresholding-Based Denoising

In this paper, an alternative denoising procedure inspired by wavelet thresholding is proposed. Some preliminary results have appeared very recently in [22]–[24] where the wavelet thresholding idea is directly applied to the EMD case. However, as will be seen later, EMD thresholding can exceed the performance achieved by wavelet thresholding only by adapting the thresholding function to the special nature of IMFs.

EMD can be interpreted as a subband-like filtering procedure resulting in essentially uncorrelated IMFs. Although the equivalent filter-bank structure is by no means predetermined and fixed as in wavelet decomposition, one can in principle perform thresholding in each IMF in order to locally exclude low-energy IMF parts that are expected to be significantly corrupted by noise. A direct application of wavelet thresholding in the EMD case translates to

$$\tilde{h}^{(i)}(t) = \begin{cases} h^{(i)}(t), & \left|h^{(i)}(t)\right| > T_i \\ 0, & \left|h^{(i)}(t)\right| \le T_i \end{cases} \tag{9}$$

for hard thresholding and to

$$\tilde{h}^{(i)}(t) = \begin{cases} \operatorname{sgn}\left(h^{(i)}(t)\right)\left(\left|h^{(i)}(t)\right| - T_i\right), & \left|h^{(i)}(t)\right| > T_i \\ 0, & \left|h^{(i)}(t)\right| \le T_i \end{cases} \tag{10}$$

for soft thresholding, where, in both thresholding cases, $\tilde{h}^{(i)}(t)$ indicates the ith thresholded IMF. The reason for adopting different thresholds T_i per mode i will become clearer in the sequel.

A generalized reconstruction of the denoised signal is given by

$$\hat{x}(t) = \sum_{k=M_1}^{M_2} \tilde{h}^{(i)}(t) + \sum_{k=M_2+1}^{L} h^{(i)}(t) \tag{11}$$

where the introduction of parameters M_1 and M_2 gives us flexibility on the exclusion of the noisy low-order IMFs and on the optional thresholding of the high-order ones, which in white Gaussian noise conditions contain little noise energy.

There are two major differences, which are interconnected, between wavelet and direct EMD thresholding (EMD-DT) shown above. First, in contrast to wavelet denoising where

thresholding is applied to the wavelet components, in the EMD case, thresholding is applied to the N samples of each IMF, which are basically the signal portion contained in each adaptive subband. An equivalent procedure in the wavelet method would be to perform thresholding on the reconstructed signals after performing the synthesis function on each scale separately. Secondly, as a consequence of the first difference, the IMF samples are not Gaussian distributed with variance equal to the noise variance, as the wavelet components are irrespective of scale. In fact, the noise contained in each IMF is colored, [5] *having different energy* in each mode. In that sense, EMD denoising is most closely related to wavelet denoising of signals corrupted by colored noise where the thresholds have to be scale dependent. In our study of thresholds, multiples of the IMF-dependent universal threshold, i.e., $T_k = C\sqrt{E_k 2\ln N}$, where C is a constant, are used. Moreover, the IMF energies can be computed directly based on the variance estimate of the first IMF using (8).

A. Thresholding Adapted to EMD Characteristics

The direct application of wavelet-like thresholding, either hard or soft, to the decomposition modes is in principle incorrect and can have catastrophic consequences for the continuity of the reconstructed signal.[6] This is because the IMFs resemble an AM/FM modulated sinusoid with zero mean. As a result, it is guaranteed that, even in a noiseless case, in any interval $\boldsymbol{z}_j^{(i)} = [z_j^{(i)} z_{j+1}^{(i)}]$, the absolute amplitude of the ith IMF, $i = 1, 2, \ldots, N$, will drop below any nonzero threshold in the proximity of the zero-crossings $z_j^{(i)}$ and $z_{j+1}^{(i)}$. In other words, based on the absolute amplitude of isolated IMF samples, it is impossible to infer for any one of them if they correspond to noise or to useful signal. However, it is possible to guess if the interval $\boldsymbol{z}_j^{(i)}$ is noise-dominant or signal-dominant based on the single extrema $h^{(i)}(r_j^{(i)})$ that correspond to this interval. If the signal is absent, the absolute value of this extrema will lie below the threshold. Alternatively, in the presence of strong signal, the extrema value can be expected to exceed the threshold. Moreover, since in each IMF the noise and the signal share the same bandwidth, the signal dominance at the extrema time instance is highly likely to be extended to all the IMF samples belonging to the specific zero-crossing interval. As a result, the newly developed EMD hard thresholding, hereafter referred to as EMD interval thresholding (EMD-IT), translates to

$$\tilde{h}^{(i)}\left(\boldsymbol{z}_j^{(i)}\right) = \begin{cases} h^{(i)}\left(\boldsymbol{z}_j^{(i)}\right), & \left|h^{(i)}\left(r_j^{(i)}\right)\right| > T_i \\ 0, & \left|h^{(i)}\left(r_j^{(i)}\right)\right| \le T_i \end{cases} \tag{12}$$

for $j = 1, 2, \ldots, N_z^{(i)}$, where $h^{(i)}(\boldsymbol{z}_j^{(i)})$ indicates the samples from instant $z_j^{(i)}$ to $z_{j+1}^{(i)}$ of the ith IMF.

After careful consideration, it can be seen that the above procedure resembles wavelet thresholding more than direct EMD thresholding because wavelet thresholding is applied to the wavelet coefficients. In fact, each coefficient is responsible for the values of a sequence of samples of the subsignal corresponding to the specific scale reconstruction. The number of these successive samples increases with scale, and it is determined by the wavelet size of support. Similarly, the number of IMF samples that are altered or not in the EMD-IT depends on the IMF order and increases as the order increases.

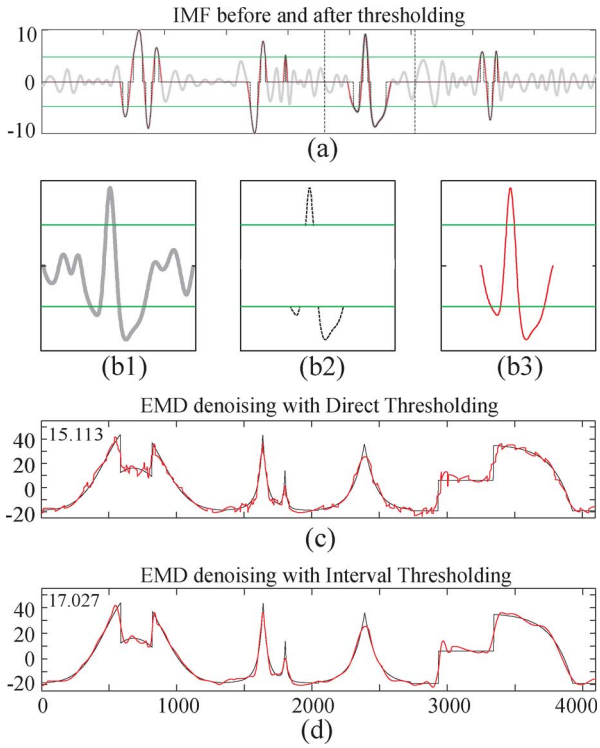

Fig. 5. Difference between direct and interval thresholding and the corresponding denoised signals.

Fig. 5(a) shows the difference between the direct and the interval EMD thresholding. As an example, the sixth IMF of the signal shown in Fig. 1 has been used. The thick light-colored line corresponds to the actual IMF, and the solid and dotted lines are associated with interval thresholding and direct thresholding, respectively. The horizontal lines indicate the plus and minus of the universal thresholding. A detail of the thresholding function applied on the IMF segment between the two vertical dashed lines in Fig. 5(a) is also depicted in Fig. 5(b1)–(b3). More specifically, in Fig. 5(b2) and (b3), we see the parts of the IMF segment that are nonzero after thresholding. Clearly, EMD-DT introduces discontinuities that can be effectively reduced by the use of EMD-IT. Fig. 5(c) and (d) shows the denoising effect when the two EMD-based thresholding methods are applied on the same noise realization of the piecewise-regular signal used in Fig. 2. We observe that EMD-IT results in higher SNR than EMD-DT. In both cases, the universal threshold is adopted, which, it should be noted, is not optimum for EMD or for wavelet thresholding, as will become apparent in the simulations section.

In a similar manner to the hard interval thresholding case, the extremum between each zero-crossing interval $[z_j^{(i)} z_{j+1}^{(i)}]$ will

[5] There is strong evidence that at least in the noise-only case, the distribution of the IMF samples is still Gaussian [21].

[6] The denoising procedure used in [11] differs from direct thresholding since the parts of the IMFs that contain useful signal are detected with the aid of a fractal dimension filter and, consequently, some of the inherent disadvantages of direct EMD thresholding can be avoided to some extent. However, this method is only efficient in denoising transient signals.

be the processing element of reference for the case of soft interval thresholding as well. Practically, the result of wavelet soft thresholding on, e.g., positive wavelet components that exceed the threshold is that the latter become reduced by an amount equal to the threshold. With respect to iterative soft thresholding, all the IMF samples that correspond to zero-crossing interval with extremum exceeding the threshold have to be reduced in a smooth way in order for the extremum to get reduced exactly by an amount equal to the threshold. Mathematically, the described soft thresholding operation yields

$$\tilde{h}^{(i)}\left(\boldsymbol{z}_j^{(i)}\right)=\begin{cases} h^{(i)}\left(\boldsymbol{z}_j^{(i)}\right)\dfrac{\left|h^{(i)}\left(r_j^{(i)}\right)\right|-T_i}{\left|h^{(i)}\left(r_j^{(i)}\right)\right|}, & \left|h^{(i)}\left(r_j^{(i)}\right)\right|>T_i \\ 0, & \left|h^{(i)}\left(r_j^{(i)}\right)\right|\le T_i \end{cases} \tag{13}$$

B. Iterative EMD Interval-Thresholding

Inspired by translation invariant wavelet thresholding, where a number of denoised versions of the signal under consideration are obtained iteratively in order to enhance the tolerance against noise by averaging them, we make an attempt to develop EMD-based denoising techniques that exploit a similar principle. Once again, the direct application of translation invariant denoising to the EMD case will not work. This arises from the fact that the wavelet components of the circularly shifted versions of the signal correspond to atoms centered on different signal instances. In the case of the data-driven EMD decomposition, the major processing components, which are the extrema, are signal dependent, leading to fixed relative extrema positions with respect to the signal when the latter is shifted. As a result, the EMD of shifted versions of the noisy signal corresponds to identical[7] IMFs sifted by the same amount. Consequently, noise averaging cannot be achieved in this way.

The different denoised versions of the noisy signal in the case of EMD can only be constructed from different IMF versions after being thresholded. Inevitably, this is possible only by decomposing different noisy versions of the signal under consideration itself. So the problem at hand translates to the following question: in which way, having a signal buried in noise, can you produce different noisy versions of the actual noise-free signal? The answer stems from within the EMD concept, exploiting the characteristics of the first IMF. We know that in white Gaussian noise conditions, the first IMF is mainly noise, and more specifically comprises the larger amount of noise compared to the rest of the IMFs. By altering in a random way the positions of the samples of the first IMF and then adding the resulting noise signal to the sum of the rest of the IMFs, we can obtain a different noisy version of the original signal. In fact, in the case where the first IMF consists of noise only, then the total noise variance of the newly generated noisy signal is the same as the original one.

The above EMD denoising technique, hereafter referred to as iterative EMD interval-thresholding (EMD-IIT), is summarized in the following steps.

[7]The IMFs can potentially be slightly different at the boundaries but only due to edge effects associated with the spline interpolation procedure.

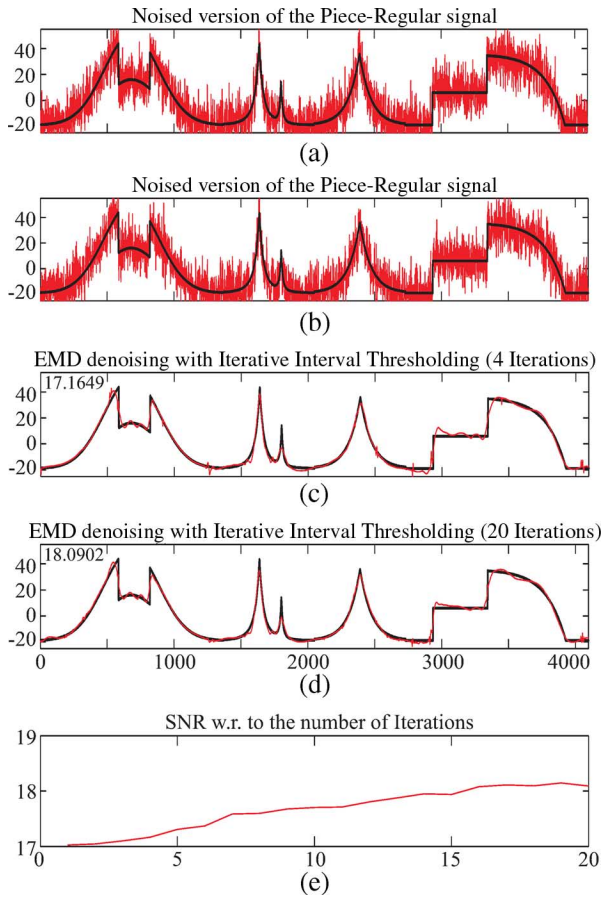

Fig. 6. (a) and (b) Two noisy versions of the piecewise-regular signal. (c) and (d) Result of the EMD-based iterative interval thresholding method using (c) four and (d) 20 iterations. (e) Achieved SNR with respect to the number of iterations.

1) Perform an EMD expansion of the original noisy signal x.
2) Perform a partial reconstruction using the last $L-1$ IMFs only, $x_p(t)=\sum_{i=2}^{L}h^{(i)}(t)$.
3) Randomly alter the sample positions of the first IMF $h_a^{(1)}(t)=\text{ALTER}(h^{(1)}(t))$.
4) Construct a different noisy version of the original signal $x_a(t)=x_p(t)+h_a^{(1)}(t)$.
5) Perform EMD on the new altered noisy signal $x_a(t)$.
6) Perform the EMD-IT denoising [(12) or (13)] on the IMFs of $x_a(t)$ to obtain a denoised version $\tilde{x}_1(t)$ of x.
7) Iterate $K-1$ times between steps 3)–6), where K is the number of averaging iterations in order to obtain k denoised versions of x, i.e., $\tilde{x}_1,\tilde{x}_2,\ldots,\tilde{x}_K$.
8) Average the resulted denoised signals $\tilde{x}(t)=(1/K)\sum_{k=1}^{K}\tilde{x}_k(t)$.

The altering function can take several forms, leading to a number of modified EMD-IIT denoising schemes. In this paper, we consider two different approaches.

- Random circulation: The samples of the first IMF are circularly shifted randomly.
- Random permutation: The samples of the first IMF randomly change positions.

Fig. 6(a) and (b) shows two different noisy versions of the piecewise-regular signal obtained by the method described in

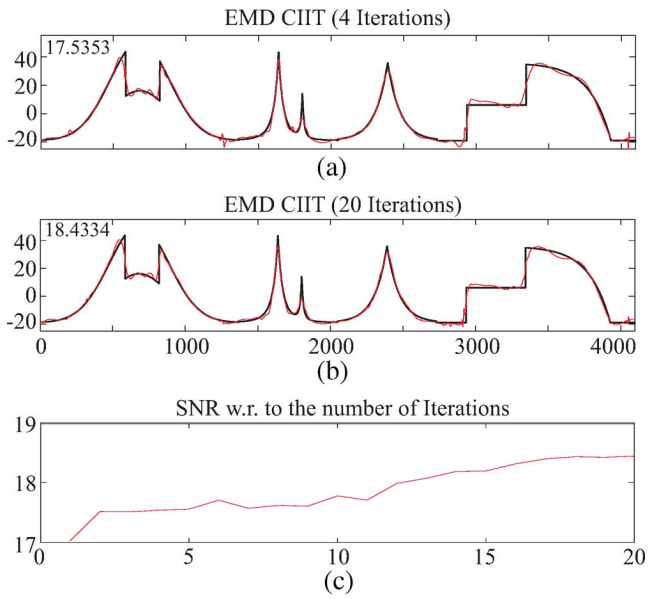

Fig. 7. (a) and (b) Denoised signals obtained with the aid of EMD-CIIT after four and 20 iterations. (c) Achieved SNR with respect to the number of iterations.

the current section when the hard EMD-IT thresholding is used. In both cases, random permutation was used as a signal altering function. The denoised signals that result from four and 20 iterations K of EMD-IIT together with the achieved SNRs are illustrated in Fig. 6(c) and (d), respectively. The noisy signal used was that described in Fig. 5. Apparently, the proposed iterative procedure has enhanced the denoising capabilities of EMD. For completeness, Fig. 6(e) shows the increment in SNR of the denoised signal with respect to the number of iterations.

C. Clear Iterative EMD Interval-Thresholding

When the noise is relatively low, enhanced performance compared to EMD-IIT denoising can be achieved with a variant called clear iterative interval-thresholding (EMD-CIIT). The need for such a modification comes from the fact that the first IMF, especially when the signal SNR is high, is likely to contain some signal portions as well. If this is the case, then by randomly altering its sample positions, the information signal carried on the first IMF will spread out contaminating the rest of the signal along its length. In such an unfortunate situation, the denoising performance will decline. In order to bypass this disadvantage of EMD-IIT it is not the first IMF that is altered directly but the first IMF after having all the parts of the useful information signal that it contains removed. The "extraction" of the information signal from the first IMF can be realized with any thresholding method, either EMD-based or wavelet-based. It is important to note that any useful signal resulting from the thresholding operation of the first IMF has to be summed with the partial reconstruction of the last $L-1$ IMFs. More specifically, steps 2) and 3) of EMD-IIT have to be replaced with the following four steps.

1) Perform an EMD expansion of the original noisy signal x.
2) Perform a thresholding operation to the first IMF of $x(t)$ to obtain a denoised version $\tilde{h}^{(1)}(t)$ of $h^{(1)}(t)$.

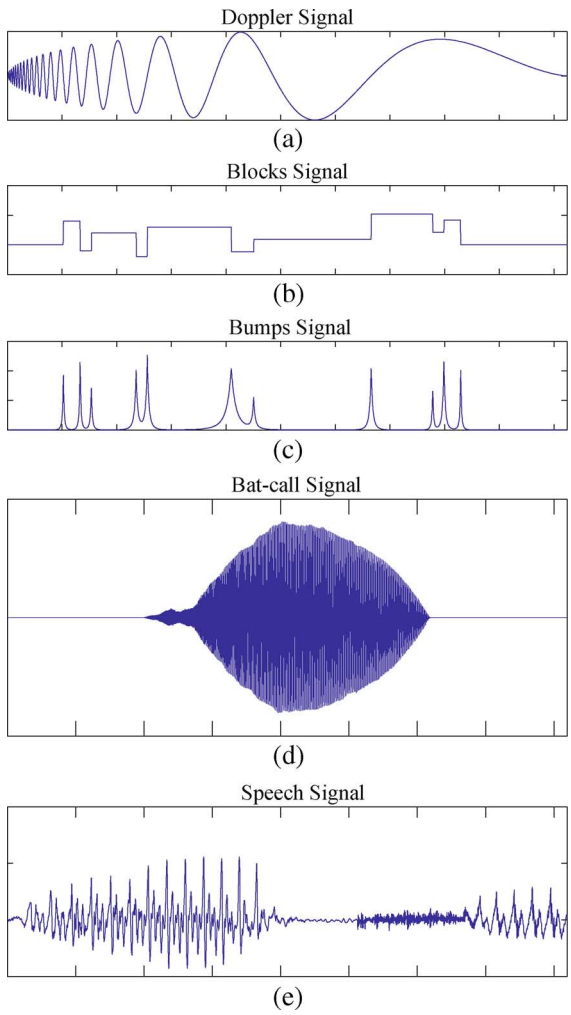

Fig. 8. Some of the signals used for validation of the denoising methods.

3) Compute the actual noise signal that existed in $h^{(1)}(t)$, $h_n^{(1)}(t) = h^{(1)}(t) - \tilde{h}^{(1)}(t)$.
4) Perform a partial reconstruction using the last $L-1$ IMFs plus the information signal contained in the first IMF, $x_p(t) = \sum_{i=2}^{L} h^{(i)}(t) + \tilde{h}^{(1)}(t)$.
5) Randomly alter the sample positions of the noise-only part of the first IMF, $h_a^{(1)}(t) = \text{ALTER}(h_n^{(1)}(t))$.

The effectiveness of the subtraction from the first IMF of any existing information signal is shown in Fig. 7. For the first IMF denoising [see step 2) above], Bayesian wavelet thresholding was used. In fact, in all the cases we have tested, the EMD interval thresholding performed similarly or worse than the Bayesian wavelet denoising when it came to the denoising of the first IMF. As a result, hereafter, whenever the EMD-CIIT is used, the adoption of the Bayesian method for the extraction of the useful signal from the first IMF is implied unless the use of a different method is explicitly mentioned.

Fig. 7(a)–(c) illustrates the same quantities as in the previous result figure and corresponds to the same noise realization with Fig. 6(c)–(e). The denoised signals that result from four and 20 iterations K of the EMD-CIIT together with the achieved SNRs are illustrated in Fig. 7(c) and (d), respectively. The noisy signal used was the same as in Fig. 5. The proposed iterative procedure

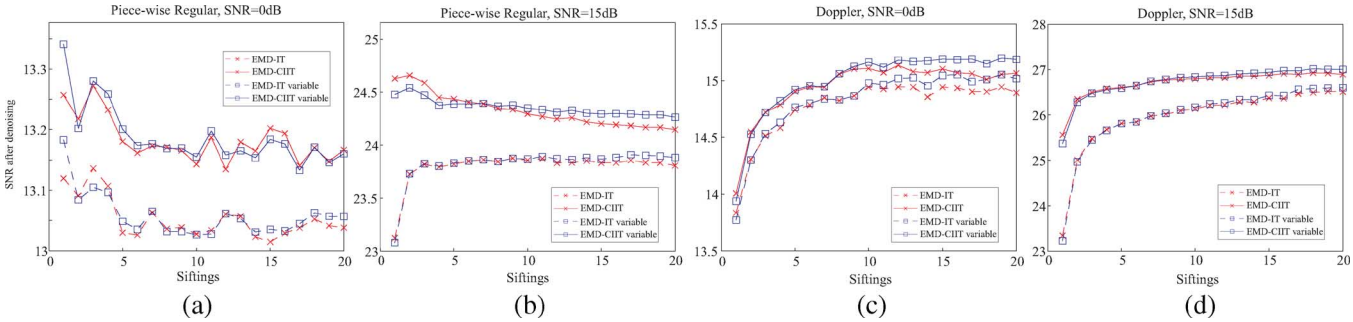

Fig. 9. SNR after denoising with respect to the number of sifting iterations in the cases of fixed or sifting-dependent IMF energy curves.

has enhanced the denoising capabilities of EMD. In both cases, random permutation was used as a signal-altering function. For completeness, Fig. 7(e) shows the increment in SNR of the denoised signal with respect to the number of iterations.

V. Simulation Results

Apart from the piecewise-regular signal, three more representative test signals shown in Fig. 8(a)–(c) have been used for validation of the proposed denoising techniques. Moreover, the best of the methods have been applied to real signals: a call signal from a bat belonging to the species *Pipistrellus Pygmaeus,*[8] shown in Fig. 8(d), and a speech signal segment illustrated in Fig. 8(e).

To start with, the effect on the denoising performance of either adopting fixed or sifting dependent IMF energy curves with respect to the number of sifting iterations is studied in Fig. 9. More specifically, the adopted performance measure is the SNR after denoising when the SNR before denoising is either 0 dB [Fig. 9(a) and (c)] or 15 dB [Fig. 9(b) and (d)] and the signals used are the piecewise regular and the Doppler signal [Fig. 8(a)], both sampled with sampling frequency that results in 2048 samples. The results shown correspond to ensemble average of 50 independent noise generalizations. The dashed curves correspond to the EMD-IT method and the solid curves to EMD-CIIT; the crosses and squares correspond to fixed and sifting-dependent IMF energy curves, respectively. A number of conclusions can be drawn. First, when the signal is regular such as the Doppler one, the larger the number of sifting iterations, the better the performance is. In contrast, when the signal has irregularities, e.g., the piece-regular signal case, the best performance (especially in the iterative EMD-CIIT method) is achieved with a relatively low number of sifting iterations. These results have been evaluated with other regular and irregular signals. In general, a balanced tradeoff between number of sifting and performance is realized with about eight sifting iterations. Secondly, it is apparent that the sifting-dependent IMF curves do not offer significant advantages over fixed curves since the performance difference never exceeds 0.2 dB. In addition, the sifting-dependent curves can even lead to slight performance deterioration in the case of EMD-CIIT when the signal has intense irregularities and a small number of sifting iterations are used. This happens because, in this case, it is very likely that large information signal portions (in the places where the irregularities exist) get extracted in the first IMF, compromising the iterative thresholding operation.

For the rest of simulation examples, each one of the artificial test signals is sampled and tested with four different sampling frequencies to generate four versions per signal, having 1024, 2048, 4096, and 8192 samples. As before, the results shown correspond to ensemble average of 50 independent noise generalizations; and in all EMD-based denoising methods, the number of sifting iterations was fixed and equal to eight. The adoption of a fixed number of sifting iterations may result in modes that do not comply with the IMF characteristics. More specifically, it is possible to find two or even more maxima (or minima) between neighboring zero-crossings. In such cases, the thresholding is naturally performed based on the largest (smallest) value of the maxima (minima) lying between consecutive zero-crossings. Moreover, the adopted performance measure is the SNR after denoising, which corresponds to SNR values of 0, 5, 10, and 15 dB before denoising. The performance results for all different methods shown correspond to hard thresholding. The conclusions drawn from the hard thresholding denoising are in general valid for the soft thresholding variants, and a discussion of the latter type of thresholding can be found at the end of the section.

Next, a thorough denoising performance evaluation of the developed and wavelet-based methods is realized using the Doppler signal [Fig. 8(a)]; then the performance of the best of the techniques when applied on the rest of the signals is examined. Fig. 10(a)–(c) depicts the performance comparison between wavelet techniques, existing and newly developed EMD-based techniques, and variants of denoising methods based on the iterative interval thresholding principle, respectively. In each graph, the performance curves correspond to SNR after denoising versus number of signal samples. They are grouped in four sets associated with 15 dB SNR before denoising (dashed-dotted curves), 10 dB SNR (dotted curves), 5 dB SNR (solid curves), and 0 dB SNR (dashed curves). The results of the wavelet-based techniques are shown in Fig. 10(a).

We observe that the best performance is achieved with the translation invariant thresholding algorithm (Hard-TI), with the Bayesian technique to follow. It is clear that the performance discrepancy between Hard-TI and Bayesian increases as the initial signal SNR increases. This trend and performance order is in general common to the rest of the signals tested. With respect to existing and newly developed EMD-based

[8]This bat-call was provided by D. Waters of the University of Leeds (http://www.fbs.leeds.ac.uk/staff/profile.php?tag=Waters).

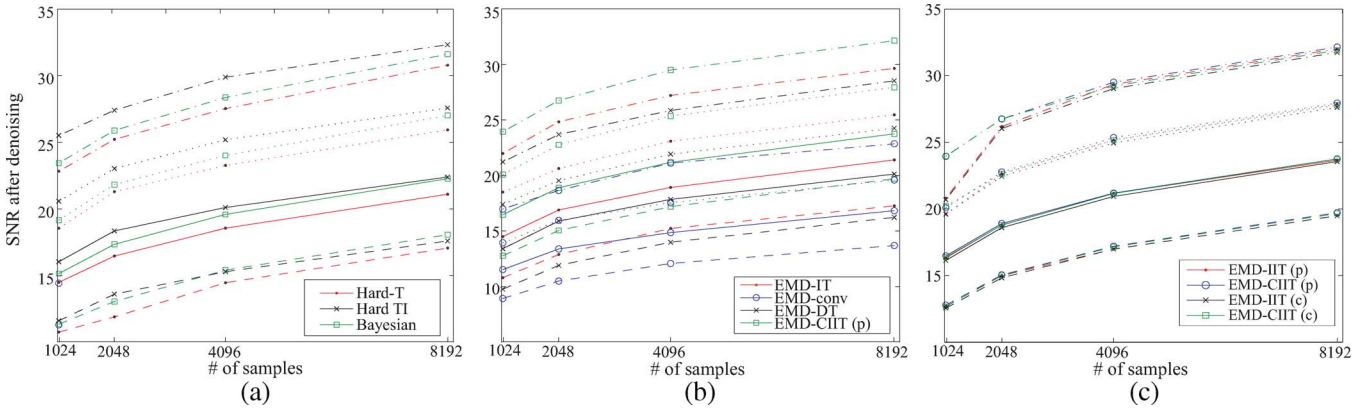

Fig. 10. Performance evaluation of the Doppler signal using wavelet and EMD-based denoising methods.

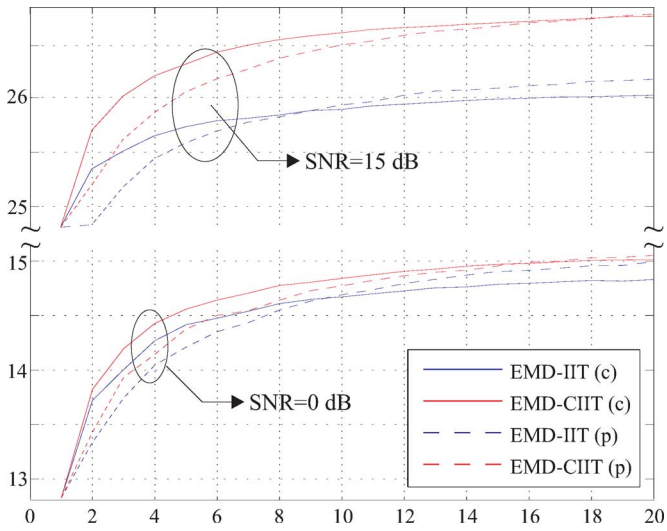

Fig. 11. Study of effect of the first IMF altering method.

methods [Fig. 10(b)], worse performance is exhibited by the conventional denoising approach (EMD-conv). The interval thresholding (EMD-IT) leads to a 1 dB improvement over direct thresholding (EMD-DT) and the incorporation of clear iterative interval thresholding with permutation altering [EMD-CIIT (p)] offers about 2 dB of extra gain. Lastly, the performance of several iterative interval (EMD-IIT) and clear iterative interval thresholding (EMD-CIIT) variants is shown in Fig. 10(c), with the number of iterations being fixed to 20. It would appear that the different methods perform in a similar way, with the EMD-CIIT denoising performing the best, especially in the case of high SNR (10 and 15 dB) and low number of samples (1024 and 2048). Moreover, the random permutation methods slightly outperform the random circulation ones.

The effect of the altering method can be further investigated with the aid of Fig. 11, where the performance of the IIT and CIIT methods when applied to the 2048 samples Doppler signal is displayed with respect to the number of iterations. We observe that in all the cases, the random circulation altering method exhibits a much faster performance improvement with respect to the number of iterations compared to random permutation. However, random permutation outperforms the random circulation after about nine or 18 iterations in the cases of IIT or CIIT, respectively. This result appears unexpected at first glance. The first IMF is roughly concentrated in the upper half-band of the spectrum, and consequently, one would expect that the averaging procedure would perform best when the altered IMFs occupy the same frequencies with the original IMF. However, this is only true for the circulation altering function. In contrast, the permutation altering inevitably leads to the redistribution of the IMF energy over the whole band. As a result, when random permutation is adopted, the denoising problem can be considered more demanding in the sense that the noise contained in the different noisy versions of the signal under consideration is no longer white. We feel that a possible explanation for the improved performance that the permutation-based denoising exhibits over the circulation-based approach would be the effect that the perturbation has on the information signal, which is contained in the first IMF. In general, the energy of the signal portions existing in the first IMF will be concentrated in time. This is true since the reason that the part of a signal is in the first IMF is its high frequency and/or high energy. This requirement is likely to be fulfilled at time intervals rather than time instances. As a result, the perturbation function will effectively spread the energy of the information signal along the full time axis, reducing its destructive effect. Indeed, the improvements achieved with the perturbation altering method are more profound in the EMD-IIT case where the first IMF is not cleared from the information signal residual.

Based on the results above, the techniques that are going to be used for a comparative performance study discussed next are EMD-IIT and EMD-CIIT, both using random permutation altering, representing the EMD-based methods; and Hard-TI and Bayesian representing the wavelet-based methods.

Fig. 12(a)–(c) shows the corresponding performance curves related to the Doppler, the piecewise-regular, and the blocks signals. It can be observed that the EMD-based methods outperform the Bayesian method for all the combinations of signal number of samples and signal SNR used. Moreover, the translation invariant hard thresholding method exhibits a significant performance improvement in the cases where the noise is relatively low (15 dB SNR), outperforming both the Bayesian and the EMD-based methods. Moreover, we see that, in general, the

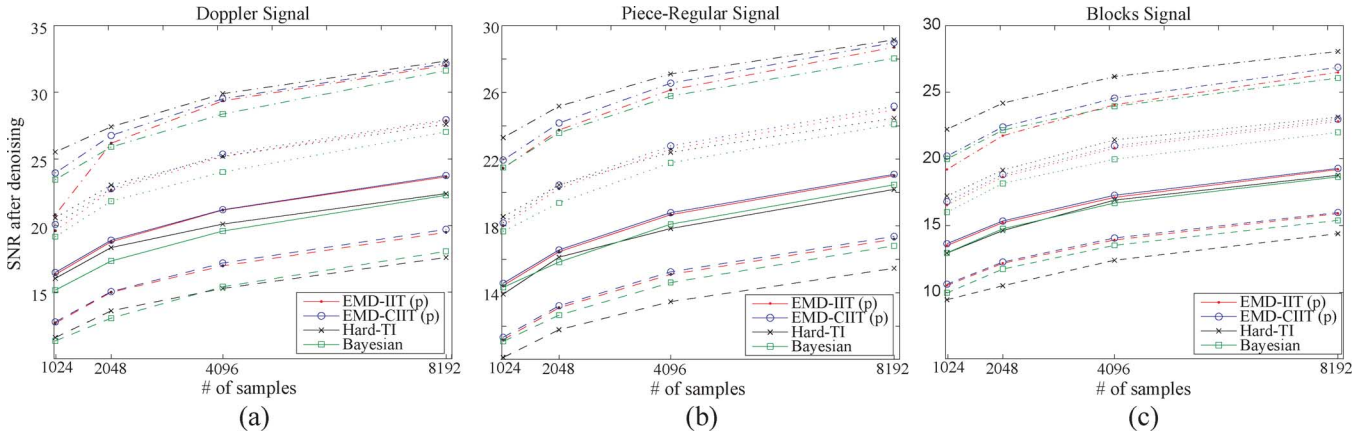

Fig. 12. Performance evaluation of EMD and wavelet-based denoising methods applied on the Doppler, piecewise-regular, and blocks signals.

TABLE I
VARIANCE OF THE SNRS OF THE DENOISED SIGNALS

Method	Doppler		Piece-Regular		Blocks		Bumps	
	0 dB	15 dB	0 dB	15 dB	0 dB	15 dB	0 dB	15 dB
EMD-CIIT (p)	0.3888	0.2319	0.2437	0.1694	0.2107	0.0953	0.1798	0.1184
Hard-TI	0.8173	0.4909	0.4396	0.2510	0.2821	0.1732	0.1887	0.0946
Bayesian	0.4358	0.2532	0.3199	0.1787	0.1722	0.1334	0.1511	0.1012

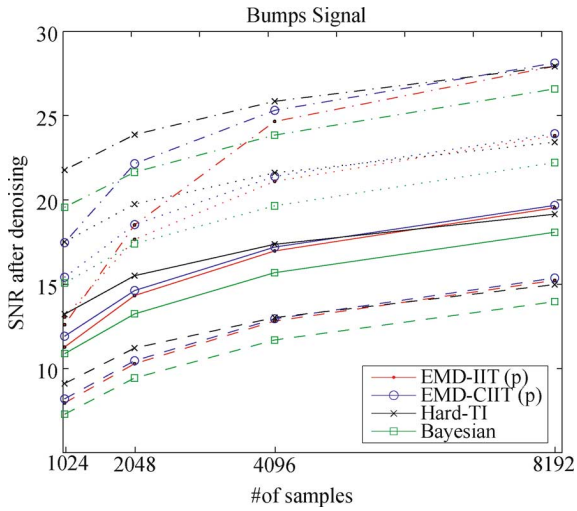

Fig. 13. Performance evaluation of EMD and wavelet-based denoising methods applied to the bumps signal.

improvement of the EMD-based methods with respect to the increment of the sampling frequency is higher than the improvement of the Hard-TI method. As a result, even in 15 dB SNR, the performance of the EMD denoising techniques tends to reach the high-performance levels of Hard-TI. A counterexample to this is the bumps signal [Fig. 8(c)], where Hard-TI outperforms the rest of the methods in all the SNRs tested with the exception of the 8192 samples case, where the EMD-CIIT method performs the best, as seen in Fig. 13. Another measure that characterizes the performance of the denoising methods is the variance of the SNR estimates, resulting from many realizations, which is shown in Table I for all the artificial signals tested with 2048 samples and for two SNR values (0 and 15 dB). The EMD-CIIT method exhibits quite a low variance, in a manner similar to the Bayesian method and in contrast to the Hard-TI, which results in higher variances—sometimes double that of the other methods. This is considered as an advantage of the EMD-CIIT-based methods.[9]

The SNR of the denoised bat and speech signal of Fig. 8(d) and (e) together with the corresponding variances are shown in Table II. With respect to the bat-call signal, the EMD-based methods outperform Hard-TI only for low SNR values. In the case of the speech segment signal, EMD denoising leads to gains between 1–0.5 dB compared to the Hard-TI method, irrespective of the noise level. Note that the sampling frequency of these signals is fixed in advance.

In all of the above simulations, the SNR values shown correspond to optimized values for the several parameters that each method uses, such as the primary resolution level for the wavelet-based denoising techniques and parameters M_1, M_2 of (11) for the EMD-based denoising. With respect to M_1, an appropriate choice stems from the lower order IMF, which contains significant portions of useful signal as it is computed by conventional EMD denoising [19]. If, for example, according to the conventional EMD approach the denoised signal has to be formed as the reconstruction of the IMFs of order J and higher (for example $J = 6$ in Fig. 4), then it has been empirically found that a very good choice of M_1 is given by

$$M_1 = \max(1, J-2). \tag{14}$$

On the other hand, a good choice of M_2 is $L-2$. In other words, the last two IMFs do not get thresholded. However, M_2 can be practically set to zero without significant effect on the performance. Lastly, for the methods where thresholding is applied, the best among the 11 thresholds was adopted for each of the different SNR/sampling frequency simulation setups. The 11

[9]EMD-IIT methods result in somewhat higher variances.

TABLE II
SNR PERFORMANCE AND VARIANCE OF EMD AND WAVELET-BASED DENOISING METHODS APPLIED ON BAT AND SPEECH SIGNAL

	Methods	SNR/Variance					
		-2 dB	0 dB	2 dB	5 dB	10 dB	15 dB
Bat-call	EMD-CIIT (c)	8.443/0.066	10.009/0.055	11.649/0.05	14.145/0.05	18.235/0.021	21.413/0.022
	EMD-CIIT (p)	8.449/0.066	10.018/0.056	11.659/0.05	14.156/0.05	18.271/0.02	21.527/0.023
	Hard-TI	7.311/0.053	9.747/0.055	11.651/0.06	14.354/0.062	20.307/0.043	23.664/0.034
	Methods	SNR/Variance					
		-2 dB	0 dB	2 dB	5 dB	10 dB	15 dB
Speech	EMD-CIIT (c)	9.504/0.061	10.704/0.046	11.932/0.033	13.718/0.021	17.061/0.02	20.730/0.017
	EMD-CIIT (p)	9.504/0.061	10.705/0.046	11.934/0.033	13.725/0.021	17.088/0.02	20.764/0.017
	Hard-TI	8.316/0.058	9.842/0.036	11.283/0.028	13.285/0.027	16.523/0.017	20.263/0.014

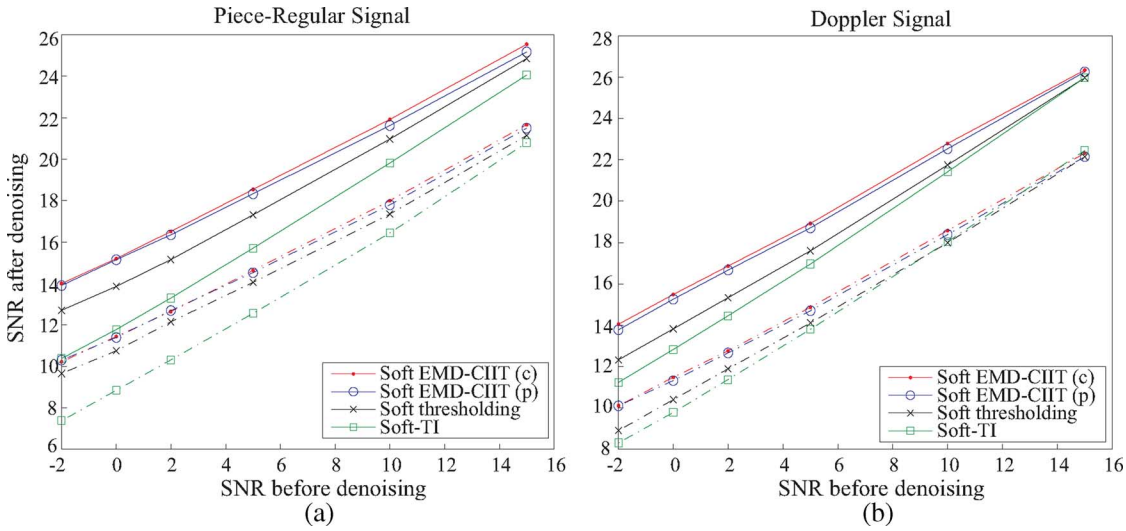

Fig. 14. Performance evaluation of EMD-base and wavelet-based soft thresholding techniques.

thresholds were calculated by multiplication of the universal threshold with the constants 0.4 up to 1.4 with steps of 0.1. It appears that in the vast majority of simulation examples and all the different simulation setups, the best threshold for the EMD-based methods was found to be between 0.6–0.8 times the universal threshold with a small performance discrepancy for any threshold between the above values. The picture is similar in the case of translation invariant thresholding, with the difference that the optimum threshold values were between 0.8 and 0.9 times the universal threshold. Based on the specific signals tested, we did not observe any noticeable increase in the sensitivity on the accuracy of the threshold selection of the EMD denoised techniques over the wavelet-based methods.

In Fig. 14, the performance of the EMD-CIIT method when it incorporates soft thresholding is compared with the performance of the ordinary and the translation invariant wavelet-based soft thresholding methods when applied to the piecewise-regular and the Doppler signal. The simulations are repeated for two different sampling frequencies, leading to 1024 (dashed curves) and 4096 (solid curves) samples. First, we observe that in the case of soft thresholding, the soft-TI exhibits inferior performance compared to standard soft thresholding. Secondly, the EMD methods outperform the wavelet thresholding ones for all of the tested SNRs. However, the trend observed in the hard thresholding case—namely, that some of the wavelet-based methods reach and even outperform the EMD methods—is still present.

When soft thresholding is used, the optimum thresholds are smaller than in the case of hard thresholding. More specifically, the EMD-CIIT methods have to use thresholds close to 0.3–0.4 times the universal threshold, while the wavelet methods perform best with thresholds close to 0.5–0.6 times the universal threshold. Moreover, parameter M_2 plays a more important role when soft thresholding is adopted. This is a result of the way that soft thresholding operates and the fact that the optimized thresholds are quite small; the thresholding of the high-order (low-frequency) IMFs can possibly lead to a power reduction of useful signal portions. As a result, it is wise to set parameter M_2 to much higher values than in the hard thresholding case, e.g., to set M_2 to five or even higher. In the SNR results of Fig. 14, parameter M_2 was not optimized but was fixed at five.

VI. CONCLUSION

In this paper, the principles of hard and soft wavelet thresholding, including translation invariant denoising, were appropriately modified to develop denoising methods suited for thresholding EMD modes. The novel techniques presented exhibit an enhanced performance compared to wavelet denoising in the cases where the signal SNR is low and/or the sampling frequency is high. These preliminary results suggest further efforts for improvement of EMD-based denoising when denoising of signals with moderate to high SNR would be appropriate.

REFERENCES

[1] Y. Kopsinis and S. McLaughlin, "Empirical mode decomposition based soft-thresholding," in *Proc. 16th Eur. Signal Process. Conf. (EUSIPCO)*, Lausanne, Switzerland, Aug. 25–29, 2008, Available: CD-ROM.

[2] Y. Kopsinis and S. McLaughlin, "Empirical mode decomposition based denoising techniques," in *Proc. 1st IAPR Workshop Cogn. Inf. Process. (CIP)*, Santorini, Greece, Jun. 9–10, 2008, pp. 42–47.

[3] N. E. Huang *et al.*, "The empirical mode decomposition and the Hilbert spectrum for nonlinear and non-stationary time series analysis," *Proc. Roy. Soc. London A*, vol. 454, pp. 903–995, Mar. 1998.

[4] L. Cohen, *Time-Frequency Analysis*. Englewood Cliffs, NJ: Prentice-Hall, 1995.

[5] P. Flandrin, G. Rilling, and P. Goncalves, "Empirical mode decomposition as a filter bank," *IEEE Signal Process. Lett.*, vol. 11, pp. 112–114, Feb. 2004.

[6] G. Rilling and P. Flandrin, "One or two frequencies? The empirical mode decomposition answers," *IEEE Trans. Signal Process.*, pp. 85–95, Jan. 2008.

[7] Y. Washizawa, T. Tanaka, D. P. Mandic, and A. Cichocki, "A flexible method for envelope estimation in empirical mode decomposition," in *Proc. 10th Int. Conf. Knowl.-Based Intell. Inf. Eng. Syst.(KES 2006)*, Bournemouth, U.K., 2006.

[8] Y. Kopsinis and S. McLaughlin, "Investigation and performance enhancement of the empirical mode decomposition method based on a heuristic search optimization approach," *IEEE Trans. Signal Process.*, pp. 1–13, Jan. 2008.

[9] Y. Kopsinis and S. McLaughlin, "Improved EMD using doubly-iterative sifting and high order spline interpolation," *EURASIP J. Adv. Signal Process.*, vol. 2008, 2008.

[10] Y. Zhang, Y. Gao, L. Wang, J. Chen, and X. Shi, "The removal of wall components in Doppler ultrasound signals by using the empirical mode decomposition algorithm," *IEEE Trans. Biomed. Eng.*, vol. 9, pp. 1631–1642, Sep. 2007.

[11] L. Hadjileontiadis, "Empirical mode decomposition and fractal dimension filter," *IEEE Eng. Med. Biol. Mag.*, pp. 30–39, Jan. 2007.

[12] B. Ning, S. Qiyu, Y. Zhihua, H. Daren, and H. Jiwu, "Robust image watermarking based on multiband wavelets and empirical mode decomposition," *IEEE Trans. Image Process.*, pp. 1956–1966, Aug. 2007.

[13] M. K. I. Molla and K. Hirose, "Single-mixture audio source separation by subspace decomposition of Hilbert spectrum," *IEEE Trans. Audio, Speech Lang. Process.*, pp. 893–900, Aug. 2007.

[14] S. Mallat, *A Wavelet Tour of Signal Processing*, 2nd ed. New York: Academic, 1999.

[15] A. Antoniadis and J. Bigot, "Wavelet estimators in nonparametric regression: A comparative simulation study," *J. Statist. Software*, vol. 6, pp. 1–83, 2001.

[16] D. L. Donoho and I. M. Johnstone, "Ideal spatial adaptation by wavelet shrinkage," *Biometrika*, vol. 81, pp. 425–455, 1994.

[17] S. Theodoridis and K. Koutroumbas, *Pattern Recognition*, 3rd ed. New York: Academic, 2006.

[18] H. C. Huang and N. Cressie, "Deterministic/stochastic wavelet decomposition for recovery of signal from noisy data," *Technometrics*, vol. 42, pp. 262–276, 2000.

[19] P. Flandrin, G. Rilling, and P. Gonçalvès, "EMD equivalent filter banks, from interpetation to applications," in *Hilbert-Huang Transform and Its Applications*, N. E. Huang and S. Shen, Eds., 1st ed. Singapore: World Scientific, 2005.

[20] Z. Wu and N. E. Huang, "A study of the characteristics of white noise using the empirical mode decomposition method," *Proc. Roy. Soc. London A*, vol. 460, pp. 1597–1611, Jun. 2004.

[21] N. E. Huang and Z. Wu, "Statistical significance test of intrinsic mode functions," in *Hilbert-Huang Transform and Its Applications*, N. E. Huang and S. Shen, Eds., 1st ed. Singapore: World Scientific, 2005.

[22] A. O. Boudraa and J. C. Cexus, "Denoising via empirical mode decomposition," in *Proc. ISCCSP 2006*, 2006.

[23] Y. Mao and P. Que, "Noise suppression and flaw detection of ultrasonic signals via empirical mode decomposition," *Rus. J. Nondestruct. Test.*, vol. 43, pp. 196–203, 2007.

[24] T. Jing-Tian, Z. Qing, T. Yan, L. Bin, and Z. Xiao-Kai, "Hilbert-huang transform for ECG de-noising," in *Proc. 1st Int. Conf. Bioinf. Biomed. Eng. (ICBBE 2007)*, 2007.

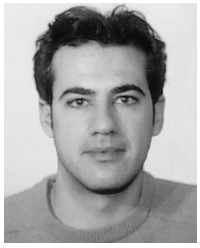

Yannis Kopsinis (M'98) was born in Patra, Greece, in 1973. He received the B.Sc. degree in informatics and the Ph.D. degree from the Department of Informatics and Telecommunications, University of Athens, Greece, in 1998 and 2003, respectively.

Since January 2004, he has been a Research Fellow with the Institute for Digital Communications, School of Engineering and Electronics, University of Edinburgh, Scotland, U.K. His research interests include channel equalization, electronic signal processing and performance evaluation for optical communication systems, time–frequency analysis, and signal decomposition.

Stephen McLaughlin (SM'04) was born in Clydebank, Scotland, U.K., in 1960. He received the B.Sc. degree in electronics and electrical engineering from the University of Glasgow, Scotland, U.K., in 1981 and the Ph.D. degree from the University of Edinburgh, Scotland, U.K., in 1989.

From 1981 to 1984, he was a Development Engineer with Barr & Stroud Ltd., Glasgow, involved in the design and simulation of integrated thermal imaging and fire control systems. From 1984 to 1986, he worked on the design and development of high-frequency data communication systems with MEL Ltd. In 1986, he joined the Department of Electronics and Electrical Engineering, University of Edinburgh, as a Research Fellow, where he studied the performance of linear adaptive algorithms in high-noise and nonstationary environments. In 1988, he joined the Academic Staff at Edinburgh, and from 1991 until 2001 he held a Royal Society University Research Fellowship to study nonlinear signal-processing techniques. In 2002, he became a Chair in Electronic Communication Systems, University of Edinburgh. His research interests lie in the fields of adaptive signal processing and nonlinear dynamical systems theory and their applications to biomedical and communication systems.

Prof. McLaughlin is a Fellow of the Institute of Engineering and Technology and the Royal Society of Edinburgh.